Applications of Circular Dichroism Spectroscopy in Studying Protein Folding, Stability, and Interaction

Preeti Gupta, Asimul Islam, Faizan Ahmad, and Md Imtaiyaz Hassan

Abstract Circular dichroism (CD) spectroscopy has been extensively used to determine the structure and folding of proteins. It provides valuable information about the protein folding phenomenon, especially the molten globule or other intermediates of the folding/unfolding pathway. This technique is beneficial in characterizing protein obtained via recombinant techniques or isolated from tissues. In addition, the effect of mutations on the folding and conformational stability of the protein can be readily assessed using CD spectroscopy. Unlike X-ray crystallography and NMR spectroscopy, the two primary powerful structure determination techniques, the ease and the requirement of low protein concentrations, make CD spectroscopy a desirable and demanding method of choice. This chapter discusses applications of CD spectroscopy in measuring protein structure and stability. The CD spectroscopic investigation of conformational changes and protein stability studied through steady-state and time-resolved CD measurements have been further highlighted. This chapter will provide a better understanding of CD spectroscopy and its uses in biomolecular studies.

1 Introduction

The characterization of recombinant proteins provides valuable information about their structure, proper folding, and stability which is invaluable for fundamental research and biopharmaceutical industries. There are many frequently used techniques to monitor the conformational changes and stability of proteins in solution,

P. Gupta · A. Islam · M. I. Hassan (✉)
Centre for Interdisciplinary Research in Basic Sciences, Jamia Millia Islamia, New Delhi, India
e-mail: mihassan@jmi.ac.in

F. Ahmad
Department of Biochemistry, Jamia Hamdard, New Delhi, India

Table 1 A comparison of CD spectroscopy, NMR spectroscopy, and X-ray crystallography

CD	NMR	X-ray crystallography
Measurements can be performed in solution	Measurements can be performed in solution	High-quality pure protein crystals are required for structure determination
0.05–1 mg/mL unlabeled protein is required depending upon the cuvette size	Structure determination typically requires a protein (labeled) concentration of 0.5 mM or greater	Approximately 10 mg of pure protein is needed to get crystals, though as little as 1 mg may now be sufficient for some proteins
Easy sample preparation	Difficult sample preparation and need for high sample purity	Difficulty in crystallizing some proteins
Molecules of any size can be studied	There is a size limitation (MWs below 40–50 kDa)	No size limitation
Does not give residue-specific information	Provide residue-specific information	Provide residue-specific information; however, protein dynamic study is not possible with the crystal
	Investigation of protein dynamics in solution is possible	Direct determination of secondary structures and especially domain movements is not possible
	Provide information on a kinetic basis, such as the internal movement of proteins over multiple time scales and their binding mechanism to ligands	Examination of small parts in the molecule is difficult
Does not provide atomic-level details	Very powerful for atomic-level structural analysis in solution	Provide atomic-level structural details in the crystalline state

such as differential scanning calorimetry (DSC), fluorescence spectroscopy, circular dichroism (CD) spectroscopy, nuclear magnetic resonance (NMR), spectroscopy, and X-ray crystallography [1–11]. Although widely used, all those techniques mentioned above have certain limitations, and hence one method is seldom enough for a detailed study of complex protein characterization. DSC requires high protein concentrations, which are challenging to achieve in the case of aggregation-prone proteins and at a bulk manufacturing scale in industries [12]. On the other hand, fluorescence spectroscopy relies on the presence of intrinsic fluorescence, making it an inefficacious technique to study proteins wherein the presence of a prosthetic group (covalently or non-covalently bound to the protein) in the close vicinity of fluorophore quenches the protein's intrinsic fluorescence. Moreover, it provides no detailed information about the global folding of the protein but instead gives an idea about the local conformational changes around the fluorophores [13, 14]. However, there are certain limitations associated with NMR and X-ray crystallography in the structural determination of proteins. The ease of CD measurements and the requirement of low protein concentrations make it a demanding technique in structural biology [7, 8]. Table 1 highlights the comparison between CD, NMR, and X-ray crystallography. This chapter aims to discuss the uses of CD spectroscopy to obtain

insights into the secondary/tertiary structures and stability/conformational dynamics of proteins. We also highlight methodological approaches in performing the CD method and data analysis tools in detail.

2 Determination of Secondary and Tertiary Structures of Proteins Using CD Spectroscopy

Far-UV CD and UV/Vis CD are absorption spectroscopy techniques that investigate the secondary structures of proteins and charge-transfer transitions in metal–protein complexes, respectively. The near-infrared CD is used to study geometric and electronic structures by probing metal $d \rightarrow d$ transitions, while the vibrational CD is used for structural studies of small organic molecules, proteins, and DNA [15]. CD utilizes the differential absorption of the right-handed and left-handed components of the circularly polarized light by the chiral molecules to study their structural aspects. The difference in the absorption of the left-handed and right-handed circularly polarized light is measured and quantified in CD experiments [16, 17]. The homochirality of amino acids imparts chirality to proteins [18]. All amino acids (except glycine) carry at least one chiral center at C_α; threonine and isoleucine have an additional chiral center at C_β [19, 20]. The CD signal is observed when a chromophore is optically active (chiral) either (1) intrinsically by its structure, (2) by being covalently linked to a chiral center, or (3) by being placed in an asymmetric environment [8]. CD is widely used to rapidly determine the secondary and tertiary structure of proteins. The CD spectrum is divided into three wavelength regions based on the electronic transitions that predominate in the given wavelength range (Fig. 1). These include:

1. The far-UV range (190–250 nm), where the contribution from peptide bonds dominates, is used to determine the secondary structure of proteins. A weak but broad $n \rightarrow \pi*$ transition region is present around 220 nm, and a stronger and sharper $\pi \rightarrow \pi*$ transition is centered at around 190 nm.
2. The near-UV range (250–300 nm), where the aromatic side chains contribute significantly, gives details about the tertiary structure of proteins.
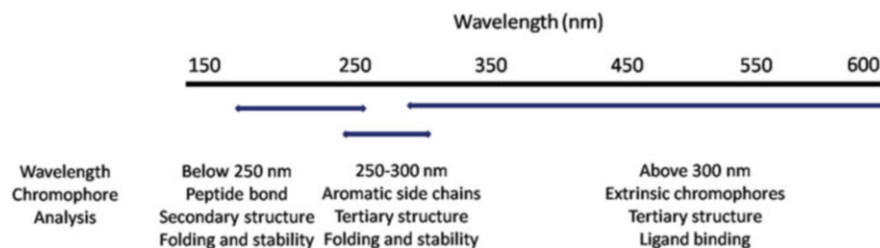

Fig. 1 CD spectral regions in proteins with their respective contributing chromophores
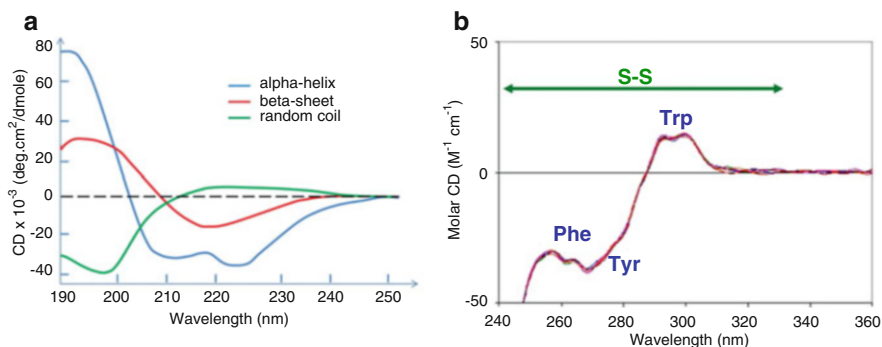
Fig. 2 (**a**) The standard far-UV spectra are associated with different secondary structures in proteins. Adapted with permission from Corrêa et al. [24]. (**b**) The near-UV CD spectra of IgG monoclonal antibody. The characteristic peaks corresponding to Trp, Tyr, and Phe signals are shown. Source: https://www.chiralabsxl.com/Circular_Dichroism/CD_App_Protein_NUV.html

3. The near UV-visible range (300–700 nm), where the extrinsic chromophores contribute, is used to monitor metal ion protein interactions [8, 21, 22].

Due to "exciton" interactions, the optical transitions of the chromophores of the polypeptide chain get split into multiple transitions when aligned in arrays. This gives characteristic CD spectra of different structural elements in the protein [6, 23]. For instance, α-helix rich proteins show two negative bands at 222 and 208 nm of comparable magnitude and a strong positive band close to 193 nm. Proteins dominated with antiparallel β-pleated sheet structure have a negative band at 218 nm and a positive band at 195 nm. Disordered proteins rich in random coil structures show a strong negative band near 195 nm [6, 24, 25]. The far-UV CD spectra of various secondary structural elements in proteins are shown in Fig. 2a.

Phenylalanine (Phe), tyrosine (Tyr), tryptophan (Trp), and disulfide bonds contribute to the near-UV CD of proteins in the wavelength region 250–300 nm. This is the region in which these chromophores absorb. The denatured protein has a weak CD signal. However, if these chromophores are buried in the folded native protein, they give strong CD signals. The intensity of the CD signal of each chromophore depends on how tightly it is held in the asymmetric environment. The near-UV CD spectrum of proteins cannot be interpreted in terms of protein structure, unlike the far-UV CD spectrum is interpreted in terms of secondary structure. However, detailed studies can decompose the CD spectrum into bands attributed to different chromophores. For instance, Trp exhibits a fine-structured peak between 290 and 305 nm. Tyr displays a peak in the range of 275–285 nm, while Phe shows a weak but intense peak at 255–270 nm. These characteristic peaks of amino acid residues emerge due to the vibronic transitions occurring in different vibrational levels of the excited state [8, 16, 26, 27]. The local tertiary structure of the protein can be used for quality control as it often reveals subtle changes from batch to batch not reflected in the far-UV region. Disulfide bonds also contribute to the CD spectrum in the near-UV region [28, 29].

Simple proteins (i.e., proteins devoid of any prosthetic group) do not absorb above 300 nm, and hence they do not exhibit CD signals in wavelengths above 300 nm. However, many prosthetic groups (non-protein chromophores or extrinsic chromophores), including flavins, pyridoxal, and heme moieties, absorb above 300 nm. In the free state, extrinsic chromophores are either achiral or present as enantiomeric mixtures, so they do not show any optical activity. However, upon interaction with the chiral environment of the protein, they generate optical activity [7, 8]. The heme group is a classic example that shows no CD signal alone but exhibits a strong positive band (Soret band) with a wavelength maximum of 412 nm when incorporated in the apoprotein of hemoglobin and myoglobin. The interaction between heme moiety and aromatic residues of the protein is thought to be the reason for heme chirality and hence the CD signal in the Soret region [30].

2.1 Servers to Estimate the Secondary Structure of Proteins from CD Data

Various web servers are available to estimate the secondary structure of the protein from CD spectroscopic data, including DichroWeb [31], BeStSel [32], and K2D3 [33]. They usually employ reference datasets consisting of a set of proteins with known structures to calculate secondary structure information that best matches the experimental (query) spectrum. The CD contribution at each wavelength is weighted, providing the correct secondary structure of the protein as the output. These servers use a range of deconvolution methods, including the simple least square method and more complicated singular value deconvolution and ridge regression method. Generally, the more diverse the components in the reference database are, the more accurate the estimation of secondary structure elements in the query spectrum [34]. It must be noted that the specialized datasets specifically designed for the integral membrane proteins are to be used for their analysis as they tend to have transitions at somewhere different wavelengths compared to soluble proteins [35].

2.1.1 DichroWeb

DichroWeb (http://dichroweb.cryst.bbk.ac.uk) is a freely available web server for determining the secondary structure of a protein based on CD and SRCD spectra. The server facilitates analyses utilizing five different algorithms, including CDSSTR, SELCON3, and VARSLEC (SVD methods with variable selection functions), CONTINLL (a regression restraint method), and K2D (a neural network method now replaced by the stand-alone K2D3 method). The server accepts data in a wide range of formats, including those output from both CD and SRCD instruments, and uses seven reference databases for structure prediction depending

upon the protein to be analyzed. It generates an output file containing calculated secondary structures, a tabular and graphical display of experimental, calculated, and difference spectra, and a goodness-of-fit parameter (normalized root mean squared deviation or NRMSD) for the analyses [34].

NRMSD is an important parameter that tells us about the correspondence between the experimental and calculated spectra and is thus used to judge the accuracy of the results. It is important to note that a low value of NRMSD is required but is insufficient to conclude the correctness of the result obtained from the analysis [34, 36]. DichroWeb highlights the importance of precise protein concentration and path length and requires the input data to be down to at least 190 nm and properly subtracted baselines before submission for accurate analysis. It also emphasizes that the best NRMSD is not always the precise solution and that the reference databases do not work well for peptides and membrane proteins [36].

2.1.2 BeStSel

BeStSel server (https://bestsel.elte.hu/index.php) is explicitly designed to analyze β-sheet rich proteins. However, it can be utilized for structural analysis of any protein class, including membrane proteins, amyloid fibrils, and protein aggregates. A comprehensive structural analysis of different secondary structure elements that includes parallel and antiparallel β-sheets and three types of twists, viz. left-handed, relaxed, and right-handed twisted sheets, is performed by the BeStSel server. Based on the structural analysis, it speculates the protein fold down to the topology level organization of the CATH protein fold database [32, 34]. Although BeStSel provides precise secondary structure estimation for a wide range of proteins, the analysis of some special structure types is unsuitable for this server. Such structures include polyproline-II helix (a characteristic structure of collagen-like fibrillar proteins), 3_{10}-helices (present in high amounts in some globular proteins), and various types of turns that are the major structural components of short peptides [32]. Also, BeStSel produces large RMSD values for intrinsically disordered proteins (IDPs) and is not a useful tool for studying this class of proteins [37].

2.1.3 K2D3

The K2D3 server (http://cbdm-01.zdv.uni-mainz.de/~andrade/k2d3/) is based on a neural network approach and a successor to the K2D method. The theoretical CD spectra of a non-redundant set of structures representing most proteins in the PDB are calculated using DichroCalc (https://comp.chem.nottingham.ac.uk/dichrocalc/). These theoretical CD spectra then serve as a reference dataset which is directly applied to predict protein secondary structure. Using the most similar CD spectra in the reference database and weighing their distances from the query spectrum, a predicted CD spectrum is generated. The output contains the query spectrum overlaid on the back-calculated spectrum along with the estimated values of

α-helix and β-sheet. No parameter that depicts the fit quality is presented in the K2D3 server. However, if the distance between the query spectrum and the most similar spectrum in the database is greater than a threshold value, a warning signal is displayed [33].

3 Determination of Conformational Changes in the Protein Using CD Spectroscopy

The conformation and structural stability are key determinants of the physiological functions of proteins. Structural perturbation in protein is one of the main reasons for the onset and progression of several diseases, including neurodegenerative disorders and cancer. For example, misfolding of α-synuclein and amyloid β leads to protein oligomerization and fibrillation, resulting in Parkinson's and Alzheimer's diseases, respectively [38, 39]. The structural alteration in the prion protein in a cell membrane environment with subsequent deposition of amyloid plaques is known to cause prion disease [40]. Genomic instability that results from mutations in crucial genes is a hallmark of almost all cancers [41]. The phenotypic outcomes of mutations on proteins include activity, binding mode and interactions, complex stability, and turnover rate.

Proteins bind to their specific targets in a precise manner, and the specificity of these interactions is predominantly defined by the structural and physicochemical properties of binding interfaces [42–44]. Any structural alteration in the protein due to genetic mutation disrupts the binding with the intracellular target, hindering the functionality of the protein. For instance, missense mutations in the BRCT domain inhibit the ability of BRCA1 for substrate recognition. Consequently, the functional role of BRCA1 in the DNA damage repair pathway is hindered and responsible for most hereditary breast and ovarian cancer cases [45]. Protein misfolding/unfolding and degradation also play crucial roles in developing lung diseases, particularly COPD (chronic obstructive pulmonary disease) and idiopathic pulmonary fibrosis and their associated clinical complications [46, 47].

Protein denaturation and aggregation are major problems during manufacturing, storage, and transport in biotechnological and pharmaceutical industries [48]. For instance, therapeutic proteins like antibodies and insulin denature in the bulk solution or at different interfaces during mass production in pharmaceutical companies. The functionality of a protein in the physiological environment or industrial applications is highly dependent on its native conformation. Thus, it is imperative to monitor conformational changes in the protein due to mutations, pH fluctuations, heat, denaturants, or binding interactions with ligands and analyze their functional consequences. CD is a reliable and convenient spectroscopic technique to detect conformational changes in the protein. Moreover, the time dependence of protein structural changes can be determined using the time-resolved CD measurements. CD is also essential in studying peptides that are not feasible by X-ray crystallography

[7]. A classic example of such a study is the switching between α-helix and β-sheet structures in prion peptides [49].

4   Analyzing the Conformational Changes in a Polypeptide Sequence upon Mutations Using CD

CD measurements can easily detect structural alterations in the protein upon mutations. Figure 3a shows the far-UV CD spectra of wild-type CopR protein and its mutants (Dim1-7). The wild-type protein shows an α-helical structure as depicted by a positive band at around 192 nm and two negative bands near 208 and 222 nm. The far-UV CD spectra of mutant proteins (Dim1, Dim3, Dim4, and Dim5) show minor deviations in the ellipticity pattern compared to the wild-type protein. This indicates that mutations did not drastically perturb the secondary structure of the proteins. In contrast, the CD spectrum of Dim6 shows a drastic reduction in α-helical content, pointing toward the significant structural perturbations upon single point mutation. The CD spectrum of Dim7 also shows conformational changes, but they are less pronounced than those in Dim6 [50].
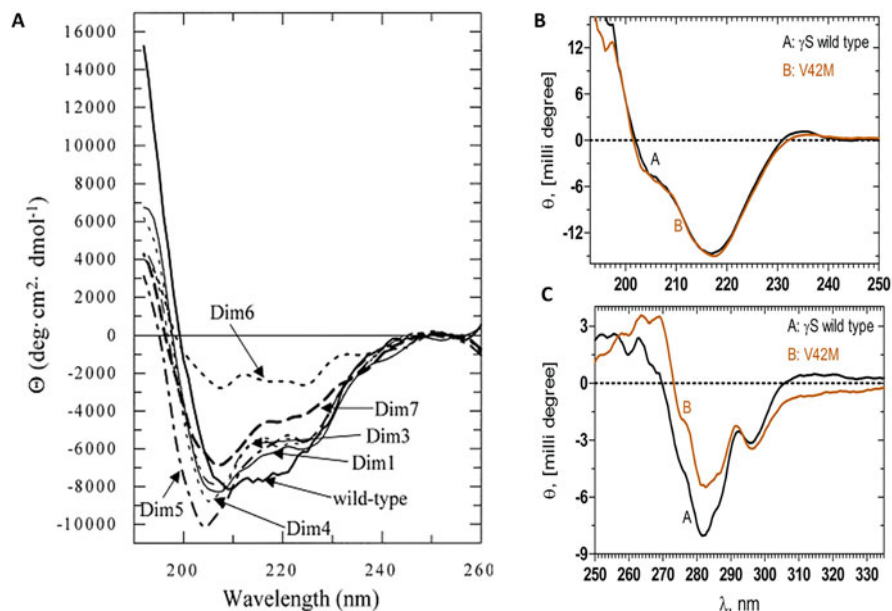

Fig. 3 A transcriptional activator protein. (**a**) Far-UV CD spectra of wild-type and mutant forms (Dim 1–7) of CopR. Adapted with permission from Steinmetzer et al. [50]. (**b**) Far-UV CD and (**c**) near-UV CD spectra of wild-type and mutant γS-crystallin (V42M). Adapted with permission from Vendra et al. [51]

Another example of monitoring mutation-induced structural changes in the protein is γS-crystallin. Figure 3b, c compares the far-UV and near-UV CD spectra of the wild-type and mutant γS-crystallin (V42M). The far-UV CD spectrum of the wild-type γS-crystallin displays two spectral bands, a negative band near 218 nm and a positive band at 195 nm, signifying the β-sheet secondary structural fold of the polypeptide chain. It should be noted that far-UV CD spectral profiles of wild-type and mutant protein were almost identical, indicating that the V42M mutation does not significantly affect the secondary structure of the protein. Strikingly, the near-UV CD spectra reveal that the tertiary structure around the aromatic residues is moderately altered in the mutant protein [51].

5 Analysis of Protein–Ligand Interactions

The binding of proteins with specific ligands such as cofactors, substrates, or regulatory molecules leads to structural changes vital for their physiological function. Such conformational changes may be monitored by the far-UV CD, near-UV CD, or both [52]. However, if the binding occurs near the aromatic amino acid residues, then small structural changes are easier to detect in the near-UV region since the CD contributions of the aromatic residues are highly sensitive to their environment. In contrast, the major structural changes in the protein's backbone are usually reflected in the far-UV CD spectrum [53, 54].

The study of ligand binding to a macromolecule is amenable if the signal from the complex is different from the sum of the signals from the components. Protein–protein interaction is a widespread and important biological regulatory phenomenon within cells. CD is a valuable technique for studying protein–protein interactions as changes occur in the secondary or tertiary structure of one or both components. The binding of small-molecule ligands such as metal ions or drugs is often accompanied by changes in the CD signal due to changes in the secondary or tertiary of the protein or the ligand. Small-molecule ligands usually have no or weak CD signal when free in solution. Still, they can show notable ellipticity when bound in the asymmetric environment of the binding pocket on the protein. Apart from protein–protein and protein–small-molecule interactions, the CD is specifically applicable to investigate protein–nucleic acid interactions as nucleic acids have strong signals in the near-UV region (250–300 nm), where proteins usually absorb weakly [55].

Human polynucleotide kinase (hPNK) acts by transferring the γ-phosphate of ATP to the 5′ ends of nucleic acids. Hence, the binding of ATP to hPNK is crucial for the proper functioning of the hPNK. Figure 4 shows the conformational changes occurring in hPNK upon binding to ATP. Two negative CD bands at 218 and 209 nm are observed in the CD spectrum of hPNK, a characteristic of the mixed α/β structure, with the band near 218 nm being attributed to the presence of β-structure in the protein. The binding of ATP to the activity of hPNK induces a substantial conformational change, as suggested by a decreased ellipticity value. The analysis of CD data indicated an increase in β-sheet structure and decreased α-helical
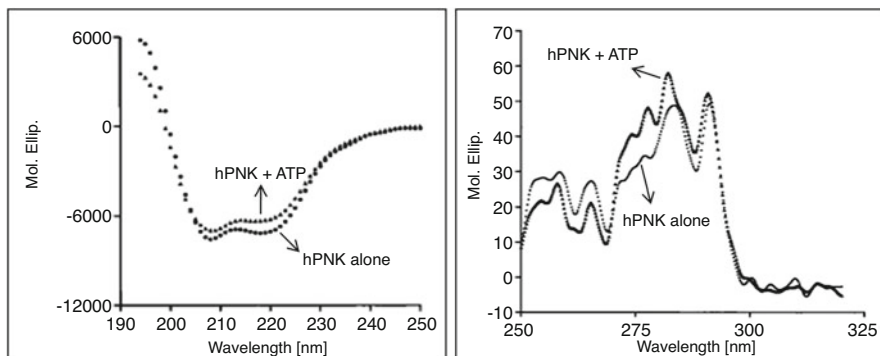
Fig. 4 Far-UV (left panel) and near-UV (right panel) CD spectra of hPNK alone (●) and in the presence of ATP (▲). Adapted with permission from Mani et al. [56]
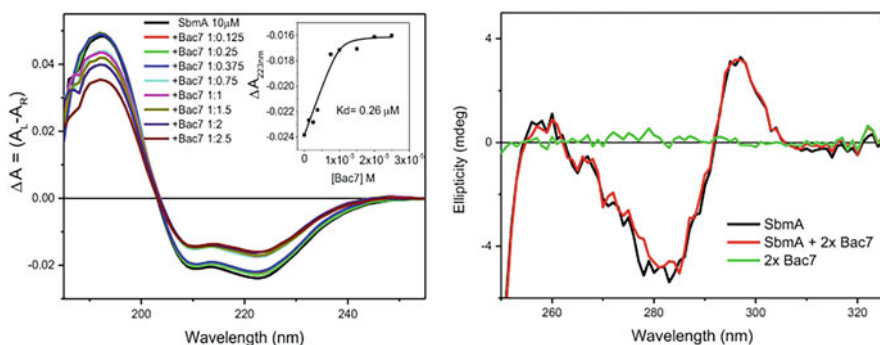

Fig. 5 Far-UV (left panel) and near-UV (right panel) CD spectra of SbmA with and without Bac7. Adapted with permission from Hussain et al. [54]. ΔA (absorption unit) = θ (ellipticity in millidegree)/3298.2

content in hPNK upon ATP binding [56]. The near-UV CD spectra also showed the perturbed environment of aromatic amino acid residues upon adding ATP. A substantial increase in the CD signal at the Trp peak near 291 nm is observed in the presence of ATP. Strikingly, two well-defined peaks attributed to tyrosine residues are observed at 284 and 278 nm instead of a broad shoulder around 279 nm in hPNK alone. The CD bands corresponding to Phe residues also show reduced ellipticity values in the apoprotein [56].

Another example where CD spectroscopy was used to monitor structural changes upon ligand binding is a bacterial inner membrane protein, SbmA, of a Gram-negative bacterium. SbmA is required to directly uptake the eukaryotic glycopeptides and antimicrobial peptides. The far-UV CD spectroscopy study showed that SbmA interacts with a proline-rich peptide, Bac7, and induces conformational changes, as revealed by the decrease in the CD signal in the wavelength range of 190–250 nm (Fig. 5). The dissociation constant (K_d) calculated after fitting the CD

data was 0.26 μM showing the high binding affinity of Bac7 to SbmA. In contrast to far-UV CD spectra, no significant changes are observed in the near-UV CD spectral range, indicating that no aromatic residues are present in close vicinity at the binding interface of protein and ligand [54].

6 Determination of Protein Folding Pathways

The proper folding of a polypeptide chain into its biologically functional native structure is one of the fundamental processes of biology. Misfolding proteins in the cellular milieu often leads to fatal human and animal diseases. In the industrial context, overexpression of recombinant proteins leads to misfolding and aggregation, causing significant loss of the final product. CD is one of the many biophysical techniques routinely used to understand various aspects of the protein folding process, including the kinetic and thermodynamic properties of folding intermediates. Investigating protein folding mechanisms in vitro also provides valuable information about cellular processes such as protein trafficking and degradation.

A CD spectrophotometer coupled with the stopped-flow system is regarded as one of the best tools to study the mechanism of unfolding and refolding of proteins. This system provides the structural data of protein during the refolding process at a sub-millisecond time scale which can be used to explore the mechanism of the protein folding pathway [57, 58]. Figure 6 shows the refolding measurements of the denatured cytochrome c in the far-UV and near-UV regions using a stopped-flow system attached to the CD spectrophotometer. The changes in the CD signal at 222 nm are faster and occur within the time scale of 200 ms, suggesting the fast refolding of the secondary structure of the protein. However, the ellipticity changes at 289 nm, reflecting the environment around aromatic residues is relatively slower. Overall, the refolding kinetics measurements indicate the brief existence of an intermediate state with a folded secondary structure and flexible aromatic residue
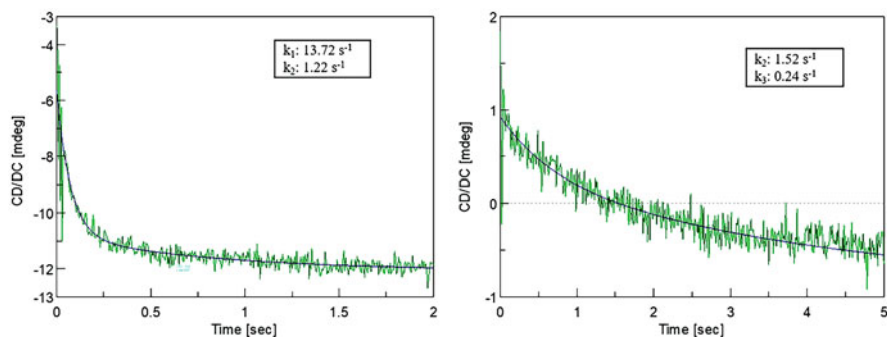

Fig. 6 Refolding kinetics of cytochrome c monitored at 222 nm (left panel) and 289 nm (right panel) using a stopped-flow CD system. Adapted with permission from [57]

side chains in the tertiary structure during the early stages of the refolding process [57].

7 Determination of Protein Stability

The stability of a protein is the fundamental property defined by the physicochemical conditions under which the protein is optimally functional. Hence, it is important to identify conditions that maximize the structural stability of the protein not only from the view of basic protein research but also to have a good yield of therapeutic proteins and other protein-based formulations in biotechnological industries. By improving the structural stability of the protein, off-pathway processes such as denaturation and aggregation could be prevented. However, it is important to note that the conditions (e.g., ionic strength, pH) that optimize the protein's physical stability might have deleterious effects on its chemical stability (e.g., deamination, oxidation). Therefore, the most stable protein formulation is achieved while considering all aspects of product quality, even with a bit of compromise with the physical and chemical stability of the protein [59]. Various methods that can be employed to measure the stability of the protein require the disruption of the native protein structure either by chemical or physical means. The conformational stability is essentially proportional to the resistance of the protein toward perturbation. The physical denaturation tools used to assess protein stability include temperature, high pressure, mechanical agitation, ultrasound, and ultraviolet radiations [60–64]. In comparison, the chemical denaturation of protein can be achieved by strong acids and bases, high concentrations of inorganic salts, salinity, organic solvents, and heavy metal salts [65–69].

7.1 Thermal Denaturation

Temperature is the most widely used tool for the physical denaturation of protein. Ideally, the thermal denaturation of a protein should be studied at its isoelectric point. However, the native protein is the least soluble at this pH, and the denatured protein is more prone to aggregation. Another disadvantage is that proteins usually get denatured far above the physiological or storage temperature. This requires long extrapolations of data to lower temperatures during thermodynamic analysis, which is often error-prone [70]. Furthermore, the thermal denaturation of proteins near their isoelectric points is usually an irreversible process that makes the calculation of stability parameters from the analysis of thermodynamic data highly unreliable and ambiguous. In such a case, physical stability rankings are presented only on T_m values, representing only a small part of the protein conformational stability curve as a function of temperature [71]. Irreversible protein denaturation is mostly followed by aggregation, affecting the accuracy of the measured T_m values [72–
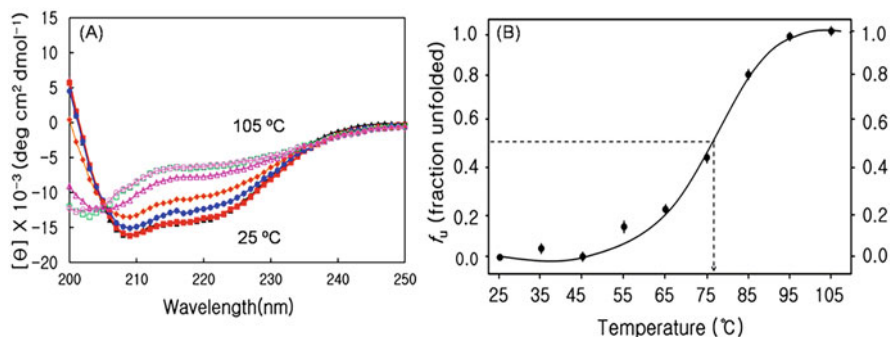
Fig. 7 Thermal unfolding of MTH1880. (**a**) Far-UV CD spectra measured at 10 °C intervals during the heating cycle (25–105 °C); 25 °C (black triangle), 45 °C (red square), 65 °C (blue circle), 75 °C (yellow square), 85 °C (pink triangle), 95 °C (green square), and 105 °C (pink circle). (**b**) A plot of fraction unfolded (f_u) derived from molar ellipticity measured at 222 nm as a function of temperature. The midpoint temperature of the unfolding transition (T_m) is 76 °C. Adapted with permission from Kim et al. [79]

74]. Additionally, the T_m value depends on the rate with which the temperature increases during the measurement, further complicating the stability extrapolations to lower temperatures.

The changes in the CD signal at a specific wavelength and as a function of temperature provide information about the thermodynamics of the protein unfolding process. The parameters retrieved from the CD thermodynamic data include the melting temperature or the midpoint temperature of the unfolding transition (T_m), the free energy of unfolding (ΔG), the van't Hoff enthalpy (ΔH) and entropy (ΔS) of unfolding, and the heat capacity changes (ΔC_P) of the unfolding transition [75]. Additionally, the analysis of CD spectra of protein acquired as a function of temperature provides information about the presence of intermediates in the folding pathway [7]. It should be noted that stability parameters obtained from the thermal denaturation curve of a protein must be validated by other experiments, such as the differential scanning calorimetry (DSC) measurements. In addition, an accurate determination of stability parameters from the analysis of optical denaturation curves depends on the temperature dependence of the pre- and post-transition baselines [76–78].

Figure 7 shows the thermal unfolding transition of MTH1880, a thermophilic protein from *Methanobacterium thermoautotrophicum*, probed by CD spectroscopy. Far-UV CD spectra were acquired with increasing temperature from 25 °C to 105 °C at an interval of 10 °C (Fig. 7a). MTH1880 shows the α-helical secondary structure in the temperature range of 25–45 °C, suggesting that the protein retains its native structural fold till 45 °C. The CD signal begins to decline continuously from 55 °C to 95 °C, where the protein is completely denatured and does not seem to show any further change in ellipticity with a further increase in the temperature. The thermal unfolding of MTH1880 follows a two-state transition unfolding pathway [79]. The raw CD data were converted into f_u, i.e., the fraction unfolded [77], which is used to

Fig. 8 Thermal unfolding of EcHUa2 followed by CD spectroscopy at 200 and 222 nm. An intermediate state is populated at around 48 °C in the melting curve. Adapted with permission from Ramstein et al. [80]
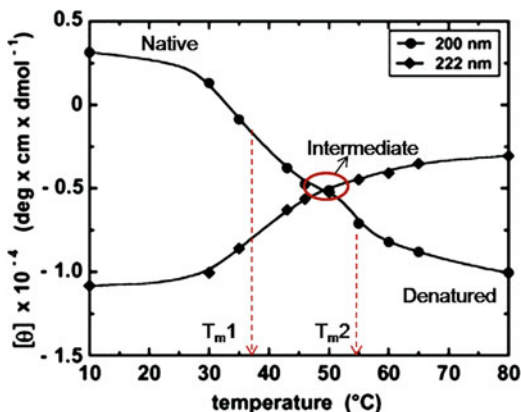
generate a f_u versus T plot (Fig. 7a). The normalized denaturation curve is fitted to the sigmoidal curve to derive thermodynamic parameters. The midpoint of unfolding transition or melting temperature (T_m) of MTH1880 was 76 °C as defined by $f_u = 0.5$.

Folding intermediates provide crucial information regarding the folding and assembly pathways. Thermal denaturation studies of protein often detect such folding/unfolding intermediates. Figure 8 shows the melting curve of *Escherichia coli* histone-like HU protein (EcHUa2) obtained by plotting the CD signals at 200 and 222 nm as a function of temperature. The thermal transition curve at 200 nm is biphasic, indicating a three-state denaturation mechanism ($N \rightarrow I \rightarrow U$) for EcHUa2 unfolding. An intermediate state is populated between N and U states at around 48 °C. The presence of two melting temperatures marks the denaturation process, i.e., 37.8 °C and 54.8 °C, corresponding to $N \rightarrow I$ and $I \rightarrow U$ transitions, respectively [80].

7.2 Chemical Denaturation

As discussed above, thermal denaturation studies of protein are often complicated and suffer from unreliable thermodynamic parameters if the unfolding process is irreversible. Different approaches are used to measure the protein stability in such a case, which employ chemical denaturants to unfold protein near-physiological temperature. Commonly used denaturants in isothermal chemical denaturation studies are urea and guanidine hydrochloride (GdnHCl) [81–83]. These chemical denaturants can prevent aggregation by keeping the unfolded protein species in stable and solubilized form, thus reversing the unfolding reaction. However, there are a few exceptions to this; for instant, low concentrations of GdnHCl fail to keep the denatured protein in the soluble form [84, 85].
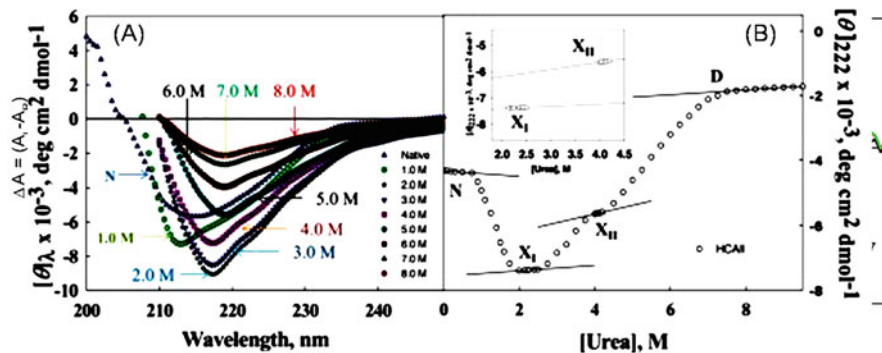
Fig. 9 Chemical denaturation of HCAII followed by CD spectroscopy. (**a**) Far-UV CD spectra of HCAII at various [Urea]. (**b**) Urea-induced denaturation is curved, followed by plotting the change in $[\theta]$ at 222 nm as a function of [Urea]. The inset shows the dependence of the optical properties of intermediates, y_{XI} and y_{XII}, on [Urea]. Adapted with permission from Wahiduzzaman et al. [95]

Measurement of typical urea (or GdnHCl)-induced denaturation curve monitored by CD involves (i) preparation of samples where the increasing concentration of denaturants are added to the protein solution followed by incubation at room temperature until the equilibrium is reached to ensure complete unfolding [59] and (ii) plotting of the CD signal at a given wavelength (θ, the raw ellipticity or $[\theta]$, the mean residue ellipticity) as a function of [denaturant], the molar concentration of the denaturant. The denaturation curve is analyzed for stability parameters, namely ΔG_D^0 (Gibbs free energy change (ΔG_D) associated with $N \leftrightarrow D$ process in the absence of the denaturant), m (dependence of ΔG_D on [denaturant]), and C_m (midpoint of denaturation curve). Analysis of the GdnHCl-induced and urea-induced denaturation curves is discussed elsewhere [86–93]. This analysis assumes that the protein denaturation is reversible. The preparation of protein samples for checking the reversibility of the denaturation by urea (or GdnHCl) is described elsewhere [86]. It should be noted that estimates of stability parameters depend on the mechanism of denaturation. However, it has to be validated whether the denaturation is a two-state process [94].

Figure 9 shows the stability studies of human carbonic anhydrase II (HCAII) employing the chemical denaturation method. Here, far-UV CD spectra of HCAII were collected at different urea concentrations (Fig. 9a). It was noted that the α-helical content increased with the addition of low concentrations of urea (0–2 M). Further increase in the urea concentration leads to the peak shift toward 218 nm, indicating the transformation of the α-helix into the β-sheet structure [95]. To obtain the denaturation curve, the molar ellipticity at 222 nm was plotted as a function of [Urea] (Fig. 9b). HCAII undergoes a cooperative triphasic unfolding profile with two distinct intermediate species (X_I and X_{II}) populated at around 2 and 4 M [Urea] on the denaturation pathway $N \leftrightarrow X_I \leftrightarrow X_{II} \leftrightarrow D$. From 0 to 2 M urea, a continuous gain in secondary structure was observed that reduced successively with
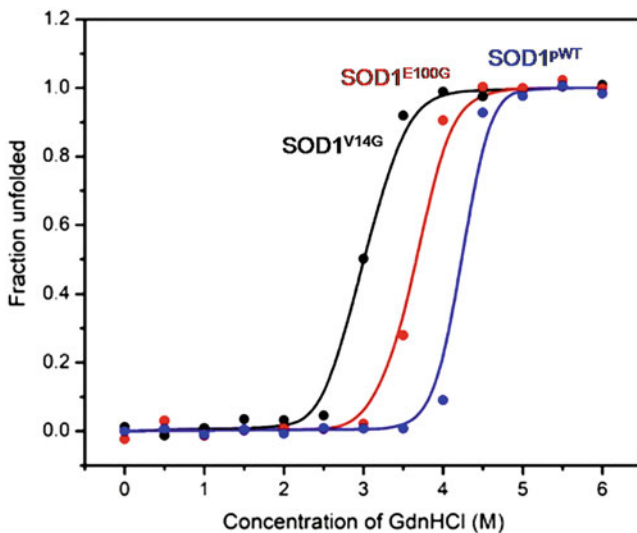
Fig. 10 GdnHCl-induced chemical denaturation curves of SOD1and its mutants monitored by CD spectroscopy. SOD1^{pWT} (blue), SOD1^{E100G} (red), and SOD1^{V14G} (black). Adapted with permission from Tompa et al. [97]

further increase in [Urea] until the protein is completely denatured. Values of the midpoint urea unfolding concentration (C_m) for transitions, $N \leftrightarrow X_I$, $X_I \leftrightarrow X_{II}$, and $X_{II} \leftrightarrow D$, were obtained after analyzing the denaturation curve, assuming that each transition curve follows a two-state mechanism ($C_{mI} = 1.33$ M, $C_{mII} = 3.25$ M, $C_{mIII} = 5.78$ M) [95].

Chemical denaturation studies provide valuable information about the destabilizing mutations that make the native protein either non-functional or prone to aggregation leading to devastating diseases [96–99]. Figure 10 shows the destabilizing effects of two single point mutations on the wild-type SOD1, whose misfolding and aggregation have been implicated in ALS. The GdnHCl-induced unfolding of SOD1^{pWT} and its mutants, SOD1^{E100G} and SOD1^{V14G}, was monitored using the far-UV CD. The denaturation curves of both wild-type and mutant proteins follow a two-state unfolding transition. The C_m values corresponding to the transition midpoints were 4.2, 3.7, and 3.0 M for SOD1^{V14G}, SOD1^{E100G}, and SOD1^{pWT}, respectively. This indicates that both mutations destabilize the wild-type SOD1protein. Although both mutations are positioned far away from the dimer interface and metal-binding site, they somehow perturb the metal loading to the active site. The partially metallated SOD1 was prone to misfolding and aggregation, causing neurodegenerative disorder [97].

8 Time-Resolved CD Measurements

CD spectroscopy has long been known as a reliable technique to determine the structural elements of proteins. It was used only to investigate the static structural properties in the past. However, it can now be employed to study protein dynamics with kinetic measurements using time-resolved CD spectroscopy. CD spectroscopy can be coupled with stopped-flow kinetic techniques to determine time dependence structural changes in the protein. The critical time-resolved CD measurements can detect events occurring on the millisecond resolution at a single wavelength [100]. The information from such studies provides mechanistic details of the protein folding phenomenon. Various excellent examples of time-resolved CD measurements are available in the literature [101–103]. Based on them, it seems that small proteins fold rapidly following a two-state transition without any detectable intermediate state(s). In contrast, larger proteins (more than 100 amino acids) usually fold via multi-state transition pathways. The native-like secondary structure is formed at the early folding stages, followed by acquiring tertiary structure interactions for larger proteins. The early intermediates formed often possess "molten globule" type characteristics.

In many experimental cases, a rapid burst phase in protein folding kinetics is reported using stopped-flow CD spectroscopy. The process occurs during the dead time of the instrument and produces an initial CD signal that differs from that expected for the unfolded protein, referred to as the burst phase. This difference in CD signal indicates that a substantial structural change occurred from D to N states during the initial burst phase [58]. An example of protein folding kinetics investigated using stopped-flow CD spectroscopy is shown in Fig. 11. The C-terminal domain (CTD) of spidroin 1 from the Ma gland (MaSp1) of the nursery web spider *Euprosthenops australis* was chemically denatured and refolded by rapid mixing into the buffer solution. A rapid burst phase of approximately 10 ms was observed within the dead time, which is beyond the detectable time resolution of the instrument. This was followed by a slow, single-exponential relaxation decay phase on the time scale of seconds [104]. To obtain the molecular details of the slow phase, the folding kinetics was measured at different protein concentrations (Fig. 11). After fitting exponential data of various protein concentrations, the time constants are almost identical within the error limits. This shows that the slow phase follows a mono-molecular folding event and is independent of protein concentration. It is also speculated that a dimeric intermediate is formed from the association of unfolded monomers during the rapid, unresolved burst phase. The event of biomolecular dimerization occurs too rapidly to be observed at the protein concentrations needed for sufficient signal in CD spectroscopy.
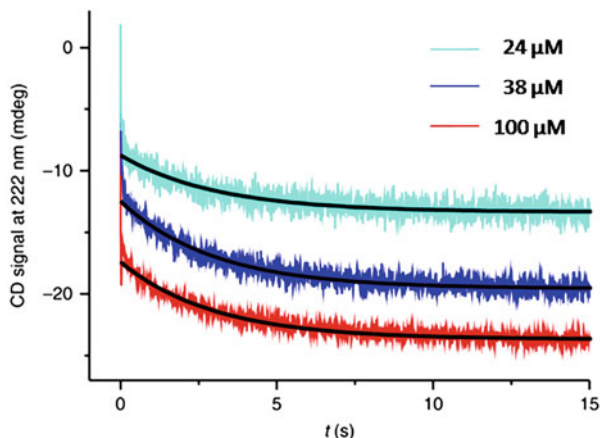
Fig. 11 Folding kinetics of CTD of spidroin 1 from the Ma gland of *Euprosthenops australis*. The far-UV CD stopped-flow spectroscopy measures the kinetic transients. Chemically denatured wild-type CTD samples at different protein concentrations (24, 38, and 100 μM) are refolded by rapid mixing into the buffer solution. The data fits the mono-exponential decay function and is depicted as a black line. Adapted with permission from Rat et al. [104]

9   Concluding Remarks

The protein folding phenomenon is of fundamental and practical importance, making the biophysical studies of protein folding and stability highly crucial. CD spectroscopy is an invaluable tool that monitors structural changes at the secondary and tertiary levels and in millisecond time resolution. It is a fast, reliable, and inexpensive technique for the initial investigation of recombinant proteins or those purified from tissues. Unlike X-ray crystallography and NMR spectroscopy, the two primary powerful structure determination techniques, the ease and the requirement of low protein concentrations, make CD spectroscopy a desirable and demanding method of choice. This chapter provides a comprehensive overview of the CD spectroscopy technique, its principle, and its applications in protein structural biology. Although CD could monitor fine structural details, more advanced and sophisticated instrumentation must be developed to detect events occurring too fast to be observed by currently available stopped-flow CD instruments. With the development of synchrotron radiation circular dichroism (SRCD) that uses high-intensity light sources, the measurement of data at lower wavelengths having more electronic transitions and thus giving more structural details has become feasible. The high signal-to-noise ratio conferred by SRCD enables the CD measurements in the presence of detergents, lipids, and other absorbing buffers.

References

1. I.B. Durowoju, K.S. Bhandal, J. Hu, B. Carpick, M. Kirkitadze, Differential scanning calorimetry—a method for assessing the thermal stability and conformation of protein antigen. J. Vis. Exp. **121**, 55262 (2017)
2. P. Gill, T.T. Moghadam, B. Ranjbar, Differential scanning calorimetry techniques: applications in biology and nanoscience. J. Biomol. Tech. **21**, 167 (2010)
3. W. Jiskoot, D. Crommelin, *Methods for Structural Analysis of Protein Pharmaceuticals* (Springer Science & Business Media, New York, 2005)
4. M.R. Eftink, The use of fluorescence methods to monitor unfolding transitions in proteins. Biophys. J. **66**, 482–501 (1994)
5. A.E. Johnson, Fluorescence approaches for determining protein conformations, interactions and mechanisms at membranes. Traffic **6**, 1078–1092 (2005)
6. N.J. Greenfield, Using circular dichroism spectra to estimate protein secondary structure. Nat. Protoc. **1**, 2876–2890 (2006)
7. S.M. Kelly, T.J. Jess, N.C. Price, How to study proteins by circular dichroism. Biochim. Biophys. Acta **1751**, 119–139 (2005)
8. S.M. Kelly, N.C. Price, The use of circular dichroism in the investigation of protein structure and function. Curr. Protein Pept. Sci. **1**, 349–384 (2000)
9. A.A. Yee, A. Savchenko, A. Ignachenko, J. Lukin, X. Xu, T. Skarina, E. Evdokimova, C.S. Liu, A. Semesi, V. Guido, A.M. Edwards, C.H. Arrowsmith, NMR and X-ray crystallography, complementary tools in structural proteomics of small proteins. J. Am. Chem. Soc. **127**, 16512–16517 (2005)
10. D.B. Singh, T. Tripathi, *Frontiers in Protein Structure, Function, and Dynamics* (Singapore, Springer Nature, 2020)
11. T. Tripathi, V.K. Dubey, *Advances in Protein Molecular and Structural Biology Methods*, 1st edn. (Academic Press, London, 2022)
12. F. van Eerden, *Differential Scanning Calorimetry and Protein Stability*, Faculty of Science and Engineering (2009)
13. H. Chosrowjan, S. Taniguchi, F. Tanaka, Ultrafast fluorescence upconversion technique and its applications to proteins. FEBS J. **282**, 3003–3015 (2015)
14. B. Bhattacharyya, S. Kapoor, D. Panda, Fluorescence spectroscopic methods to analyze drug–tubulin interactions, in *Methods in Cell Biology*, ed. by L. Wilson, J.J. Correia, (Academic Press, Cambridge, MA, 2010), pp. 301–329
15. A.A.T. Naqvi, T. Mohammad, G.M. Hasan, M.I. Hassan, Advancements in docking and molecular dynamics simulations towards ligand-receptor interactions and structure-function relationships. Curr. Top. Med. Chem. **18**, 1755–1768 (2018)
16. D.M. Rogers, S.B. Jasim, N.T. Dyer, F. Auvray, M. Réfrégiers, J.D. Hirst, Electronic circular dichroism spectroscopy of proteins. Chem **5**, 2751–2774 (2019)
17. G. Büyükköroğlu, D.D. Dora, F. Özdemir, C. Hızel, Techniques for protein analysis, in *Omics Technologies and Bio-Engineering*, ed. by D. Barh, V. Azevedo, (Academic Press, London, 2018), pp. 317–351
18. J. Skolnick, H. Zhou, M. Gao, On the possible origin of protein homochirality, structure, and biochemical function. Proc. Natl. Acad. Sci. **116**, 26571–26579 (2019)
19. C.-L. Towse, G. Hopping, I. Vulovic, V. Daggett, Nature versus design: the conformational propensities of D-amino acids and the importance of side chain chirality. Protein Eng. Des. Sel. **27**, 447–455 (2014)
20. Y. Jeong, H.W. Kim, J. Ku, J. Seo, Breakdown of chiral recognition of amino acids in reduced dimensions. Sci. Rep. **10**, 16166 (2020)
21. M. Mulkerrin, *Protein Structure Analysis Using Circular Dichroism* (VCH Publishers, New York, 1996)

22. N.J. Greenfield, Biomacromolecular applications of circular dichroism and ORD, in *Encylopedia of Spectroscopy and Spectrometry*, ed. by J.C. Lindon, G.E. Trantor, J.L. Holmes, (Academic Press, Oxford, 1999), pp. 117–130

23. N. Sreerama, R.W. Woody, Computation and analysis of protein circular dichroism spectra. Methods Enzymol. **383**, 318–351 (2004)

24. D.H.A. Corrêa, C.H.I. Ramos, The use of circular dichroism spectroscopy to study protein folding, form and function. Afr. J. Biochem. Res. **3**, 164–173 (2009)

25. N. Greenfield, Using circular dichroism collected as a function of temperature to determine the thermodynamics of protein unfolding and binding interactions. Nat. Protoc. **1**, 2527–2535 (2006)

26. A. Rodger, Near UV protein CD, in *Encyclopedia of Biophysics*, ed. by G.C.K. Roberts, (Springer, Berlin, 2013), pp. 1694–1694

27. A. Naiyer, B. Khan, A. Hussain, A. Islam, M.F. Alajmi, M.I. Hassan, M. Sundd, F. Ahmad, Stability of uniformly labeled (^{13}C and ^{15}N) cytochrome C and its L94G mutant. Sci. Rep. **11**, 6804 (2021)

28. J.M. Antosiewicz, D. Shugar, UV-Vis spectroscopy of tyrosine side-groups in studies of protein structure. Part 2: selected applications. Biophys. Rev. **8**, 163–177 (2016)

29. A. Mcauley, J. Jacob, C.G. Kolvenbach, K. Westland, H.J. Lee, S.R. Brych, D. Rehder, G.R. Kleemann, D.N. Brems, M. Matsumura, Contributions of a disulfide bond to the structure, stability, and dimerization of human IgG1 antibody CH3 domain. Protein Sci. **17**, 95–106 (2008)

30. M. Nagai, Y. Nagai, K. Imai, S. Neya, Circular dichroism of hemoglobin and myoglobin. Chirality **26**, 438–442 (2014)

31. L. Whitmore, B.A. Wallace, Protein secondary structure analyses from circular dichroism spectroscopy: methods and reference databases. Biopolymers **89**, 392–400 (2008)

32. A. Micsonai, F. Wien, É. Bulyáki, J. Kun, É. Moussong, Y.H. Lee, Y. Goto, M. Réfrégiers, J. Kardos, BeStSel: a web server for accurate protein secondary structure prediction and fold recognition from the circular dichroism spectra. Nucleic Acids Res. **46**, W315–W322 (2018)

33. C. Louis-Jeune, M.A. Andrade-Navarro, C. Perez-Iratxeta, Prediction of protein secondary structure from circular dichroism using theoretically derived spectra. Proteins **80**, 374–381 (2012)

34. A.J. Miles, R.W. Janes, B.A. Wallace, Tools and methods for circular dichroism spectroscopy of proteins: a tutorial review. Chem. Soc. Rev. **50**, 8400–8413 (2021)

35. B.A. Wallace, R.W. Janes, *Modern Techniques for Circular Dichroism and Synchrotron Radiation Circular Dichroism Spectroscopy* (IOS Press, Amsterdam, 2009)

36. L. Whitmore, B. Wallace, DICHROWEB, an online server for protein secondary structure analyses from circular dichroism spectroscopic data. Nucleic Acids Res. **32**, W668–W673 (2004)

37. J.C. Ezerski, P. Zhang, N.C. Jennings, M.N. Waxham, M.S. Cheung, Molecular dynamics ensemble refinement of intrinsically disordered peptides according to deconvoluted spectra from circular dichroism. Biophys. J. **118**, 1665–1678 (2020)

38. H.A. Lashuel, C.R. Overk, A. Oueslati, E. Masliah, The many faces of α-synuclein: from structure and toxicity to therapeutic target. Nat. Rev. Neurosci. **14**, 38–48 (2013)

39. G.-f. Chen, T.-h. Xu, Y. Yan, Y.-r. Zhou, Y. Jiang, K. Melcher, H.E. Xu, Amyloid beta: structure, biology and structure-based therapeutic development. Acta Pharmacol. Sin. **38**, 1205–1235 (2017)

40. C. Soto, N. Satani, The intricate mechanisms of neurodegeneration in prion diseases. Trends Mol. Med. **17**, 14–24 (2011)

41. S. Negrini, V.G. Gorgoulis, T.D. Halazonetis, Genomic instability—an evolving hallmark of cancer. Nat. Rev. Mol. Cell Biol. **11**, 220–228 (2010)

42. M. Vihinen, Functional effects of protein variants. Biochimie **180**, 104–120 (2021)

43. M. Li, A. Goncearenco, A.R. Panchenko, Annotating mutational effects on proteins and protein interactions: designing novel and revisiting existing protocols. Methods Mol. Biol. **1550**, 235–260 (2017)
44. M. Li, M. Petukh, E. Alexov, A.R. Panchenko, Predicting the impact of missense mutations on protein–protein binding affinity. J. Chem. Theory Comput. **10**, 1770–1780 (2014)
45. S.L. Clark, A.M. Rodriguez, R.R. Snyder, G.D.V. Hankins, D. Boehning, Structure-function of the tumor suppressor BRCA1. Comput. Struct. Biotechnol. J. **1**, e201204005 (2012)
46. K.L. Bradley, C.A. Stokes, S.J. Marciniak, L.C. Parker, A.M. Condliffe, Role of unfolded proteins in lung disease. Thorax **76**, 92–99 (2021)
47. S.G. Kelsen, The unfolded protein response in chronic obstructive pulmonary disease. Ann. Am. Thorac. Soc. **13**(Suppl 2), S138–S145 (2016)
48. C. Mueller, U. Altenburger, S. Mohl, Challenges for the pharmaceutical technical development of protein coformulations. J. Pharm. Pharmacol. **70**, 666–674 (2018)
49. K.S. Satheeshkumar, R. Jayakumar, Conformational polymorphism of the amyloidogenic peptide homologous to residues 113–127 of the prion protein. Biophys. J. **85**, 473–483 (2003)
50. K. Steinmetzer, A. Hillisch, J. Behlke, S. Brantl, Transcriptional repressor CopR: amino acids involved in forming the dimeric interface. Proteins **39**, 408–416 (2000)
51. V.P.R. Vendra, S. Chandani, D. Balasubramanian, The mutation V42M distorts the compact packing of the human gamma-S-Crystallin molecule, resulting in congenital cataract. PLoS One **7**, e51401 (2012)
52. G. Siligardi, R. Hussain, S.G. Patching, M.K. Phillips-Jones, Ligand- and drug-binding studies of membrane proteins revealed through circular dichroism spectroscopy. Biochim. Biophys. Acta Biomembr. **1838**, 34–42 (2014)
53. F.M. Assadi-Porter, J. Radek, H. Rao, M. Tonelli, Multimodal ligand binding studies of human and mouse G-coupled taste receptors to correlate their species-specific sweetness tasting properties. Molecules **23**, 2531 (2018)
54. R. Hussain, G. Siligardi, Characterisation of conformational and ligand binding properties of membrane proteins using synchrotron radiation circular dichroism (SRCD). Adv. Exp. Med. Biol. **922**, 43–59 (2016)
55. A. Podjarny, A. Dejaegere, B. Kieffer, *Biophysical Approaches Determining Ligand Binding to Biomolecular Targets: Detection, Measurement and Modelling* (Royal Society of Chemistry, Cambridge, 2011)
56. R.S. Mani, F. Karimi-Busheri, C.E. Cass, M. Weinfeld, Physical properties of human polynucleotide kinase: hydrodynamic and spectroscopic studies. Biochemistry **40**, 12967–12973 (2001)
57. S. Anwar, A. Shamsi, T. Mohammad, A. Islam, M.I. Hassan, Targeting pyruvate dehydrogenase kinase signaling in the development of effective cancer therapy. Biochim. Biophys. Acta Rev. Cancer **1876**, 188568 (2021)
58. H. Roder, K. Maki, H. Cheng, Early events in protein folding explored by rapid mixing methods. Chem. Rev. **106**, 1836–1861 (2006)
59. H. Svilenov, U. Markoja, G. Winter, Isothermal chemical denaturation as a complementary tool to overcome limitations of thermal differential scanning fluorimetry in predicting physical stability of protein formulations. Eur. J. Pharm. Biopharm. **125**, 106–113 (2018)
60. W. Messens, J. Van Camp, A. Huyghebaert, The use of high pressure to modify the functionality of food proteins. Trends Food Sci. Technol. **8**, 107–112 (1997)
61. Y. Matsuura, M. Takehira, Y. Joti, K. Ogasahara, T. Tanaka, N. Ono, N. Kunishima, K. Yutani, Thermodynamics of protein denaturation at temperatures over 100 °C: CutA1 mutant proteins substituted with hydrophobic and charged residues. Sci. Rep. **5**, 15545 (2015)
62. N. Dhanapati, M. Ishioroshi, I. Yoshida, K. Samejima, Effects of mechanical agitation, heating and pH on the structure of bovine alpha lactalbumin. Anim. Sci. Technol. **68**, 545–554 (1997)
63. V. De Leo, L. Catucci, A.E. Di Mauro, A. Agostiano, L. Giotta, M. Trotta, F. Milano, Effect of ultrasound on the function and structure of a membrane protein: the case study of

photosynthetic reaction center from Rhodobacter sphaeroides. Ultrason. Sonochem. **35**, 103–111 (2017)

64. J.H. Clark, The denaturation of egg albumin by ultra-violet radiation. J. Gen. Physiol. **19**, 199–210 (1935)

65. R. Dahiya, T. Mohammad, M.F. Alajmi, M.T. Rehman, G.M. Hasan, A. Hussain, M.I. Hassan, Insights into the conserved regulatory mechanisms of human and yeast aging. Biomol. Ther. **10**, 1–27 (2020)

66. S. Singh, C. Tyagi, I.A. Rather, J.S.M. Sabir, M.I. Hassan, A. Singh, I.K. Singh, Molecular modeling of chemosensory protein 3 from Spodoptera litura and its binding property with plant defensive metabolites. Int. J. Mol. Sci. **21**, 1–15 (2020)

67. P. Gupta, F.I. Khan, S. Roy, S. Anwar, R. Dahiya, M.F. Alajmi, A. Hussain, M.T. Rehman, D. Lai, M.I. Hassan, Functional implications of pH-induced conformational changes in the Sphingosine kinase 1. Spectrochim. Acta A Mol. Biomol. Spectrosc. **225**, 117453 (2020)

68. F. Ahmad, Protein stability from denaturation transition curves. Indian J. Biochem. Biophys. **28**, 168–173 (1991)

69. F. Ahmad, *Measuring the Conformational Stability of Enzymes in the Thermostability of Enzymes* (Narosa Publishing House: India, New Delhi, 1993), pp. 95–112

70. D. Matulis, J.K. Kranz, F.R. Salemme, M.J. Todd, Thermodynamic stability of carbonic anhydrase: measurements of binding affinity and stoichiometry using thermofluor. Biochemistry **44**, 5258–5266 (2005)

71. E. Freire, A. Schön, B.M. Hutchins, R.K. Brown, Chemical denaturation as a tool in the formulation optimization of biologics. Drug Discov. Today **18**, 1007–1013 (2013)

72. A. Azuaga, C. Dobson, P. Mateo, F. Conejero-Lara, Unfolding and aggregation during the thermal denaturation of streptokinase. Eur. J. Biochem. **269**, 4121–4133 (2002)

73. A. Schön, B.R. Clarkson, M. Jaime, E. Freire, Temperature stability of proteins: analysis of irreversible denaturation using isothermal calorimetry. Proteins **85**, 2009–2016 (2017)

74. J.M. Sanchez-Ruiz, Theoretical analysis of Lumry-Eyring models in differential scanning calorimetry. Biophys. J. **61**, 921–935 (1992)

75. D.C. Rees, A.D. Robertson, Some thermodynamic implications for the thermostability of proteins. Protein Sci. **10**, 1187–1194 (2001)

76. A. Sinha, S. Yadav, R. Ahmad, F. Ahmad, A possible origin of differences between calorimetric and equilibrium estimates of stability parameters of proteins. Biochem. J. **345**, 711–717 (2000)

77. S. Yadav, F. Ahmad, A new method for the determination of stability parameters of proteins from their heat-induced denaturation curves. Anal. Biochem. **283**, 207–213 (2000)

78. F. Ahmad, Protein folding: estimates of stability parameters from heat-induced conformational transition curves of proteins. PINSA **68**, 385–390 (2002)

79. H. Kim, S. Kim, Y. Jung, J. Han, J.-H. Yun, I. Chang, W. Lee, Probing the folding-unfolding transition of a thermophilic protein, MTH1880. PLoS One **11**, e0145853 (2016)

80. J. Ramstein, N. Hervouet, F. Coste, C. Zelwer, J. Oberto, B. Castaing, Evidence of a thermal unfolding dimeric intermediate for the Escherichia coli histone-like HU proteins: thermodynamics and structure. J. Mol. Biol. **331**, 101–121 (2003)

81. E. Freire, A. Schon, B. Hutchins, R. Brown, Chemical denaturation as a tool in the formulation optimization of biologics. Drug Discov. Today **18**, 1007 (2013)

82. F.I. Khan, P. Gupta, S. Roy, N. Azum, K.A. Alamry, A.M. Asiri, D. Lai, M.I. Hassan, Mechanistic insights into the urea-induced denaturation of human sphingosine kinase 1. Int. J. Biol. Macromol. **161**, 1496–1505 (2020)

83. P. Gupta, F.I. Khan, D. Ambreen, D. Lai, M.F. Alajmi, A. Hussain, A. Islam, F. Ahmad, M.I. Hassan, Investigation of guanidinium chloride-induced unfolding pathway of sphingosine kinase 1. Int. J. Biol. Macromol. **147**, 177–186 (2020)

84. R. Singh, M.I. Hassan, A. Islam, F. Ahmad, Cooperative unfolding of residual structure in heat denatured proteins by urea and guanidinium chloride. PLoS One **10**, e0128740 (2015)

85. F. Ahmad, P. McPhie, Thermodynamics of the denaturation of pepsinogen by urea. Biochemistry **17**, 241–246 (1978)
86. F. Ahmad, C.C. Bigelow, Estimation of the free energy of stabilization of ribonuclease a, lysozyme, alpha-lactalbumin, and myoglobin. J. Biol. Chem. **257**, 12935–12938 (1982)
87. F. Ahmad, C.C. Bigelow, Estimation of the stability of globular proteins. Biopolymers **25**, 1623–1633 (1986)
88. F. Ahmad, S. Yadav, S. Taneja, Determining stability of proteins from guanidinium chloride transition curves. Biochem. J. **287**, 481–485 (1992)
89. R. Gupta, S. Yadav, F. Ahmad, Protein stability: urea-induced versus guanidine-induced unfolding of metmyoglobin. Biochemistry **35**, 11925–11930 (1996)
90. T. Tripathi, S. Rahlfs, K. Becker, V. Bhakuni, Structural and stability characteristics of a monothiol glutaredoxin: glutaredoxin-like protein 1 from plasmodium falciparum. Biochim. Biophys. Acta **1784**, 946–952 (2008)
91. T. Tripathi, B.K. Na, W.M. Sohn, K. Becker, V. Bhakuni, Structural, functional and unfolding characteristics of glutathione S-transferase of plasmodium vivax. Arch. Biochem. Biophys. **487**, 115–122 (2009)
92. T. Tripathi, A. Röseler, S. Rahlfs, K. Becker, V. Bhakuni, Conformational stability and energetics of plasmodium falciparum glutaredoxin. Biochimie **92**, 284–291 (2010)
93. T. Tripathi, Calculation of thermodynamic parameters of protein unfolding using far-ultraviolet circular dichroism. J. Protein. Proteomics **4**, 85–91 (2013)
94. H. Rahaman, M.K.A. Khan, M.I. Hassan, A. Islam, A.A. Moosavi-Movahedi, F. Ahmad, Evidence of non-coincidence of normalized sigmoidal curves of two different structural properties for two-state protein folding/unfolding. J. Chem. Thermodyn. **58**, 351–358 (2013)
95. D.M. Wahiduzzaman, M.A. Haque, D. Idrees, M.I. Hassan, A. Islam, F. Ahmad, Characterization of folding intermediates during urea-induced denaturation of human carbonic anhydrase II. Int. J. Biol. Macromol. **95**, 881–887 (2017)
96. P. Gupta, P. Mahlawat, S. Deep, Effect of disease-linked mutations on the structure, function, stability and aggregation of human carbonic anhydrase II. Int. J. Biol. Macromol. **143**, 472–482 (2020)
97. D.R. Tompa, S. Kadhirvel, Far positioned ALS associated mutants of cu/Zn SOD forms partially metallated, destabilized misfolding intermediates. Biochem. Biophys. Res. Commun. **516**, 494–499 (2019)
98. S. Boopathy, T.V. Silvas, M. Tischbein, S. Jansen, S.M. Shandilya, J.A. Zitzewitz, J.E. Landers, B.L. Goode, C.A. Schiffer, D.A. Bosco, Structural basis for mutation-induced destabilization of profilin 1 in ALS. Proc. Natl. Acad. Sci. **112**, 7984–7989 (2015)
99. M. Andreasen, S.B. Nielsen, K. Runager, G. Christiansen, N.C. Nielsen, J.J. Enghild, D.E. Otzen, Polymorphic fibrillation of the destabilized fourth fasciclin-1 domain mutant A546T of the transforming growth factor-β-induced protein (TGFBIp) occurs through multiple pathways with different oligomeric intermediates. J. Biol. Chem. **287**, 34730–34742 (2012)
100. Y.G. Thomas, I. Szundi, J.W. Lewis, D.S. Kliger, Microsecond time-resolved circular dichroism of rhodopsin photointermediates. Biochemistry **48**, 12283–12289 (2009)
101. C.M. Dobson, Protein folding and misfolding. Nature **426**, 884–890 (2003)
102. C.N. Pace, Conformational stability of globular proteins. Trends Biochem. Sci. **15**, 14–17 (1990)
103. R.L. Baldwin, G.D. Rose, How the hydrophobic factor drives protein folding. Proc. Natl. Acad. Sci. **113**, 12462–12466 (2016)
104. C. Rat, J.C. Heiby, J.P. Bunz, H. Neuweiler, Two-step self-assembly of a spider silk molecular clamp. Nat. Commun. **9**, 4779 (2018)